

This work was written as part of one of the author's official duties as an Employee of the United States Government and is therefore a work of the United States Government. In accordance with 17 U.S.C. 105, no copyright protection is available for such works under U.S. Law. Access to this work was provided by the University of Maryland, Baltimore County (UMBC) ScholarWorks@UMBC digital repository on the Maryland Shared Open Access (MD-SOAR) platform.

Please provide feedback

Please support the ScholarWorks@UMBC repository by emailing scholarworks-group@umbc.edu and telling us what having access to this work means to you and why it's important to you. Thank you.

Resonant and nonresonant funneling through plasmonic gratings in the limit of the aperture width approaching zero

Cite as: Appl. Phys. Lett. **104**, 021103 (2014); <https://doi.org/10.1063/1.4861850>

Submitted: 30 September 2013 . Accepted: 27 December 2013 . Published Online: 13 January 2014

M. J. Bloemer, N. Mattiucci, G. D'Aguanno, R. Trimm, and N. Akozbek



View Online



Export Citation



CrossMark

ARTICLES YOU MAY BE INTERESTED IN

Broadband Brewster transmission through 2D metallic gratings

Journal of Applied Physics **112**, 094317 (2012); <https://doi.org/10.1063/1.4764334>

Broadband transmission enhancement of acoustic waves through a hybrid grating

Applied Physics Letters **100**, 191908 (2012); <https://doi.org/10.1063/1.4714719>

Three-dimensional broadband and high-directivity lens antenna made of metamaterials

Journal of Applied Physics **110**, 044904 (2011); <https://doi.org/10.1063/1.3622596>

Lock-in Amplifiers
up to 600 MHz



Watch



Resonant and nonresonant funneling through plasmonic gratings in the limit of the aperture width approaching zero

M. J. Bloemer,^{1,a)} N. Mattiucci,² G. D'Aguanno,² R. Trimm,³ and N. Akozbek²

¹Department of the Army, C. M. Bowden Laboratory, Redstone Arsenal, Alabama 35898, USA

²Aegis Technologies, Inc., 410 Jan Davis Drive, Huntsville, Alabama 35809, USA

³Miltec Corporation, 678 Discovery Drive, Huntsville, Alabama 35806, USA

(Received 30 September 2013; accepted 27 December 2013; published online 13 January 2014)

We experimentally and theoretically investigate electromagnetic funneling in thick plasmonic gratings as the aperture size approaches zero. Both resonant and nonresonant funneling mechanisms were observed to provide near unity transmission for aperture widths of $\sim \lambda/100$. As the apertures become smaller, the resonant funneling process enters into a region of strong absorption followed by complete reflection. In sharp contrast, the broadband, nonresonant funneling mechanism continues to transmit energy at high levels for screens of $<1\%$ open area and apertures sizes as small as $\lambda/1500$ before finally transitioning to a completely absorbing state without any abatement of the funneling into the apertures. © 2014 AIP Publishing LLC.

[<http://dx.doi.org/10.1063/1.4861850>]

Pendry has shown that thick metal gratings (thickness on the order of a wavelength or thicker) can support resonant transmission modes for p-polarized light.¹ These resonance modes are a combination of Transverse ElectroMagnetic (TEM) waveguide modes in the slit that do not have a cutoff thickness and Fabry-Perot resonances due to the abrupt boundaries at the air/grating interface. The resonances are insensitive to the angle of incidence and provide near unity transmittance under the condition of weak penetration of the electric field into the metal. More recently, a broadband nonresonant transmission mechanism through metal gratings was theoretically predicted^{2,3} and experimentally observed at microwave⁴ and THz frequencies.⁵ This nonresonant transmission spans a huge frequency range from dc to frequencies that have wavelengths on the order of the grating period and is a result of impedance matching of the incident p-polarized radiation and the surface of the grating. This impedance matching condition known as the “plasmonic Brewster angle” is independent of the thickness of the grating and independent of the geometrical detail of the slit except at the grating surface. For a grating, the Brewster angle is defined by the relationship $\tan \theta_B = d/w$, where d is the grating period and w is the aperture width. The resonant and nonresonant enhanced optical transmission mechanisms have also been demonstrated in 2D gratings and were shown to be robust at all azimuthal angles of incidence.⁶

In Ref. 7, it was noted that from a metamaterial point of view, 1D metallic gratings are equivalent to a high index dielectric with an effective index of refraction $n_{\text{eff}} = d/w$ and an effective length $l_{\text{eff}} = l(w/d)$. Since the slits can be extremely narrow, the result is a metamaterial with a very large index of refraction. An experimental demonstration of a metallic grating with an effective index of 5.5 and low loss was presented in Ref. 8. From the metamaterial perspective, the 1D grating is a high index solid etalon that supports

Fabry-Perot modes (resonant funneling) and a broadband Brewster angle transmission (nonresonant funneling). Remarkably, the high index etalon/grating can act as a waveguide and supports guided modes along the width of the grating, propagating transverse to the grating slits.⁷

In this Letter, we theoretically and experimentally explore resonant and nonresonant transmission through the grating as the aperture width approaches zero to determine the limits of the funneling process. The experiments were performed at microwave frequencies of 8–40 GHz on a grating having apertures as small as $25 \mu\text{m}$ (Fig. 1). This corresponds to an aperture width of $\lambda/1500$ at 8 GHz. For the $25 \mu\text{m}$ aperture size, the open area of the grating was a mere 0.78% to determine whether all of the impinging radiation could efficiently funnel through these extremely narrow apertures that are sparsely spaced and possibly produce a low loss

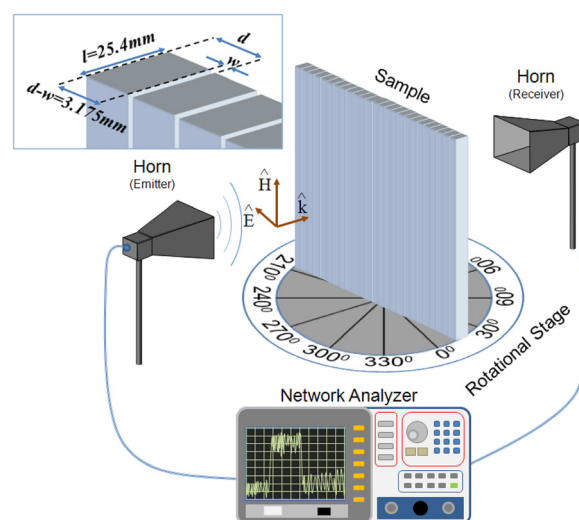


FIG. 1. Schematic of the grating and the experimental setup. The grating thickness is $l = 25.4 \text{ mm}$, the period is $d = 3.20 \text{ mm}$, and the aperture width is $w = 25 \mu\text{m}$. Transmission measurements were performed in an anechoic chamber over the range of 8–40 GHz from normal incidence up to 85° .

^{a)} Author to whom correspondence should be addressed. Electronic mail: mark.j.bloemer.civ@mail.mil

metamaterial with an index of refraction of $n_{\text{eff}} > 100$. Similar measurements have been performed on gratings with apertures of 50, 400, and 1,500 μm .⁴

In the microwave, the wavevector of the TEM guided mode in a metal/air/metal waveguide is usually considered equal to the vacuum wavevector $\beta_{\text{WG}} = k_0$ because of the negligible penetration of the electric field into the metal. Here, however, we explore the regime of extremely narrow apertures which causes a non-negligible field penetration inside the metal and increased losses. As a consequence, the pure TEM waveguide mode actually becomes a “plasmonic” transverse magnetic (TM) mode with increased dissipation and slow wave properties, i.e., $\text{Re}(\beta_{\text{WG}}) > k_0$ and $\text{Im}(\beta_{\text{WG}}) > 0$. Fig. 2 shows the refractive index of the guided mode $n_{\text{WG}} = \text{Re}(\beta_{\text{WG}})/k_0$ and its propagation length $L_p = (2\text{Im}(\beta_{\text{WG}}))^{-1}$ for an Al/air/Al waveguide as function of the air thickness w at a frequency of 10 GHz. The aluminum dispersion in the microwave region has been calculated using a lossy Drude model whose parameters (plasma frequency and damping) were chosen according to the experimental data reported in Ref. 9. The figure shows that n_{WG} starts to depart from 1 for air thickness less than 100 μm and, at the same time, L_p decreases, as one may expect. In these extreme situations, the losses associated with the field propagation inside each slit can no longer be neglected.

According to Ref. 2, below the first diffraction order, the grating can be viewed as an effective homogeneous material with same physical length of the real grating $l_{\text{eff}} = l$ and with effective metamaterial (MM) parameters (permittivity and permeability) given by the following equations:

$$\varepsilon_{\text{MM}} = \varepsilon_w d/w, \quad \mu_{\text{MM}} = w(\beta_{\text{WG}}^2/k_0^2 + \sin^2 \vartheta)/d\varepsilon_w, \quad (1)$$

where ε_{MM} and μ_{MM} are the electric permittivity and magnetic permeability of the metamaterial slab, ϑ is the incident angle, ε_w is the dielectric constant of the material filling the slits ($\varepsilon_w = 1$ our case), k_0 is the vacuum wavevector, and β_{WG} is the wave-vector of the fundamental TM guided mode of the parallel plate metal/air/metal waveguides which the grating is made of. Note, incidentally, that the homogenization procedure of Eq. (1) from Ref. 2 is roughly equivalent to a

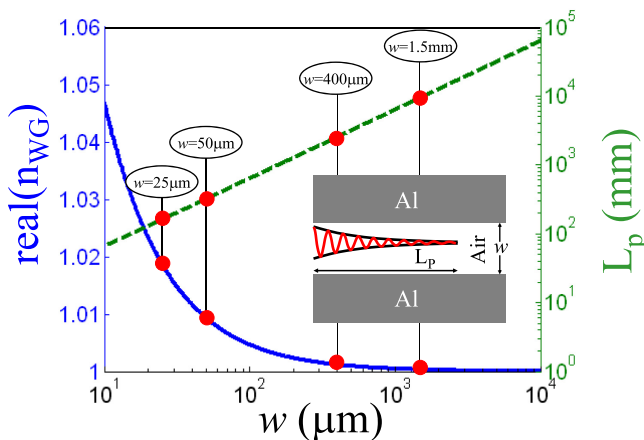


FIG. 2. Propagation length and waveguide effective index $n_{\text{WG}} = \beta_{\text{WG}}/k_0$, for the TEM mode of an Al/air/Al planar waveguide as a function of air thickness at a frequency of 10 GHz. A waveguide effective index of $n_{\text{WG}} > 1$ indicates penetration of the electric field into the metal.

non-magnetic MM slab with effective length $l_{\text{eff}} = l(w/d)$ and effective refractive index $n_{\text{eff}} = (d/w) (\beta_{\text{WG}}/k_0)$ as in Ref. 7.

Fig. 3 shows the theoretical p-polarized transmittance, reflectance, and absorbance of an Al grating at normal incidence (resonant funneling) and at the Brewster angle (nonresonant funneling) as a function of frequency and slit width calculated according to the homogenization theory of Ref. 2. The grating is 25.4 mm thick, each Al bar is 3.175 mm wide, and the period varies with the slit width. The most striking feature of the plots in Fig. 3 is the very high transmittance at the Brewster angle for the entire range of frequencies and for very narrow slits. For aperture widths of only 50 μm or $\lambda/750$ at 8 GHz, the predicted transmittance at the Brewster angle

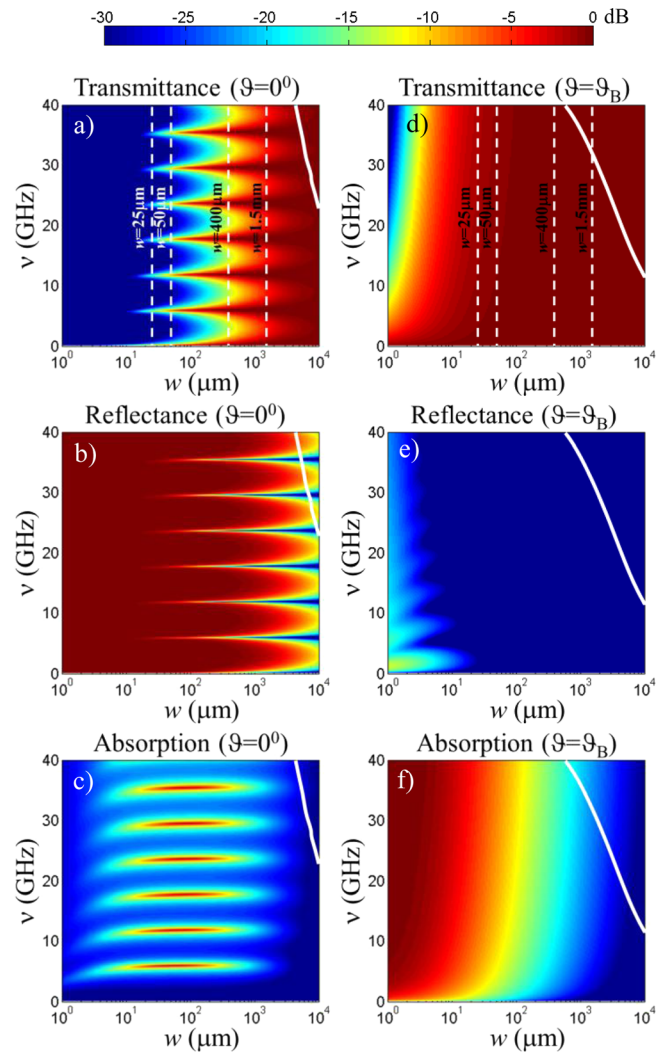


FIG. 3. Left panels (a)–(c) show the theoretical transmittance, reflectance, and absorbance of an Al grating at normal incidence (resonant funneling) as a function of the aperture width and frequency. Right panels (d)–(f) show the same but at the Brewster angle of incidence (nonresonant funneling). The grating is 25.4 mm thick and the Al bars are each 3.175 mm wide. The aperture width ranges from 1 μm to 10 mm and the frequency range is 100 MHz to 40 GHz. The straight dashed lines in the upper panels correspond to aperture widths of 25, 50, 400, and 1500 μm , where experimental data are available. The solid curved white line in the plots is the boundary for the onset of first order diffraction. The data above the white line are when first order diffraction is present and the homogenization procedure is no longer valid. The reflection at the Brewster angle is very low over all frequencies, and all aperture widths and the corresponding transmittance is large. The data plotted in the panels on the right, (d)–(f), track the Brewster angle which varies depending on the aperture width and period.

is 90% and corresponds to an effective index of refraction $n_{\text{eff}} = 65$. The Brewster angle transmittance drops to 10% only for extremely small apertures of $\sim 3 \mu\text{m}$, while the reflection remains less than 1% for apertures down to $1 \mu\text{m}$. This remarkable result indicates that metallic gratings efficiently collect all the energy impinging at the Brewster angle for open areas of the grating as little as 1 part in 3000. Under these extreme conditions, metals can no longer be considered perfect conductors, and the absorption at the Brewster angle can become significant at the higher frequencies.

The resonant funneling behaves quite differently than the nonresonant funneling. Notably, the reflection for small apertures of less than $10 \mu\text{m}$ is quite large and uniform across the entire frequency range. The grating now behaves as if it were a uniform sheet of metal. At this aperture width, the resonant funneling has essentially ceased and all of the impinging radiation is reflected. For more moderate aperture widths of $10\text{--}100 \mu\text{m}$, the absorption is substantial and the transmittance drops rapidly with decreasing aperture width. As the resonant cavity losses increase with reduced aperture size, the funneling into the cavities decreases until the losses are so large that the funneling ceases altogether. These losses are not present at the Brewster angle and are due to the long dwell time for radiation at the Fabry-Perot resonant frequencies. For apertures $> 100 \mu\text{m}$, resonant funneling is very efficient and the transmittance is near unity.

The absorption losses shown in Fig. 3 are directly related to the thickness of the grating by way of the waveguide propagation losses shown in Fig. 2. It would be possible to funnel and transmit radiation through a grating having $10 \mu\text{m}$ apertures with virtually no losses if the grating thickness was reduced to several millimeters. Thinner gratings would provide low loss metamaterials with effective indices of $n_{\text{eff}} > 100$.

The grating and experimental setup have been described in detail elsewhere.⁴ Briefly, the grating consists of 300 flat aluminum stock bars, with each bar having nominal dimensions of $0.3175 \times 2.54 \times 60 \text{ cm}$ (Fig. 4). The bars were held in place with threaded rods at the top and bottom of the grating. Apertures were made with $25 \mu\text{m}$ thick plastic shim stock between the bars. The surface roughness of the Al bars

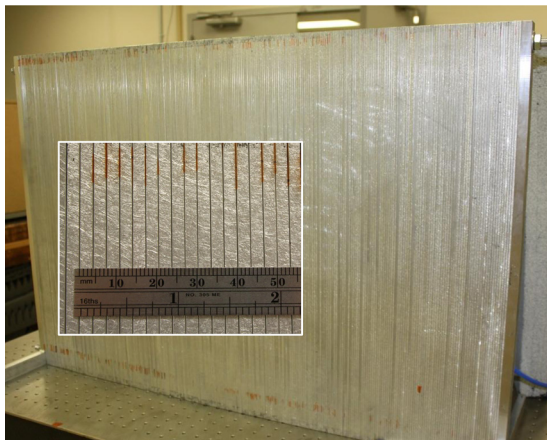


FIG. 4. Photograph of the grating. The grating was 90 cm wide, 60 cm high, and 2.54 cm thick. The large area facilitated measurements at steep angles of up to 85° . Orange colored shim stock is partially visible near the top and bottom of the grating. The corners of the Al bars were slightly rounded.

was measured with a profilometer and was on the order of $7 \mu\text{m}$. While the average spacing between the Al bars was $25 \mu\text{m}$, the flex in each bar allowed the aperture to vary to a minimum value set by the surface roughness and resulted in a range of aperture widths of approximately $15\text{--}35 \mu\text{m}$ as measured by a “feeler gauge.” The surface roughness and the aperture variations were not considered in the theoretical models. The grating was placed on a rotational stage between two microwave horns which were connected to a network analyzer (Agilent E8363C). Two sets of horns were used in the measurements having ranges of $8\text{--}18 \text{ GHz}$ and $18\text{--}40 \text{ GHz}$.

The experimental and theoretical transmittance of an Al grating with $25 \mu\text{m}$ apertures are plotted in Fig. 5. It was difficult to measure the transmittance beyond an angle of 85°

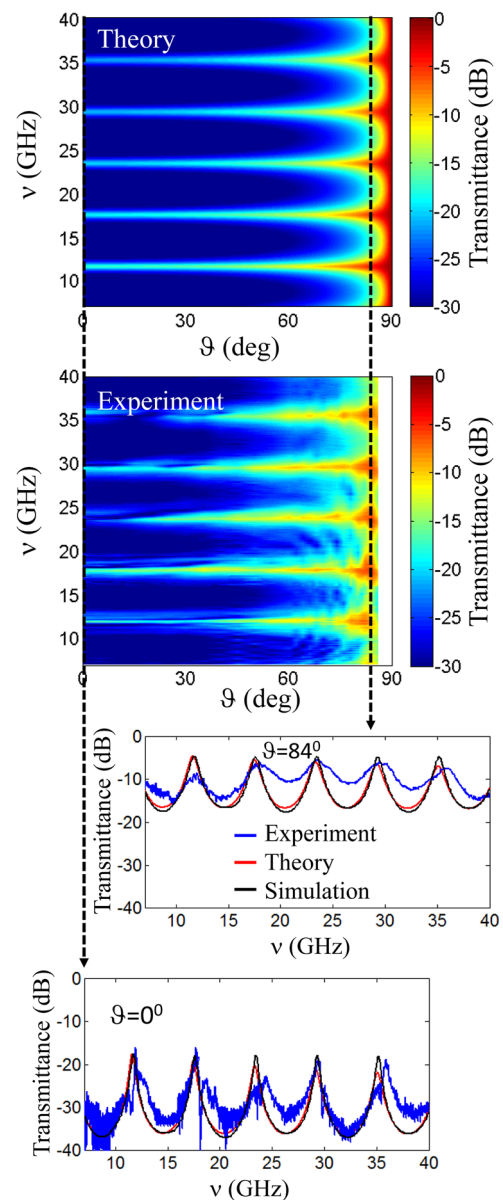


FIG. 5. Theoretical and experimental transmittance as a function of incident angle and frequency of an Al grating having an aperture width of $25 \mu\text{m}$, thickness of 25.4 mm , and period of 3.20 mm . Also shown are 2D plots extracted from the 3D plots at normal incidence and at 84° for a more direct comparison. Open area of the grating is 0.78% and the aperture width is $\lambda/1500$ at 8 GHz .

without a much larger grating surface. As a check for microwave leakage around the grating at 85° , the back of the grating was covered with Al foil and the received signal was reduced to the background noise level of -40 dB. At normal incidence, the maximum transmittance due to resonant funneling through the grating is $\sim 1\%$. In contrast, at 84° , the transmittance reaches nearly 50% even though we are several degrees away from the Brewster angle of 89.55° . At this steep angle of 84° , the maxima in the transmittance agree very well with the predictions and illustrate the onset of nonresonant transmission. The experimental minima are higher at steep angles due to the fact that the impinging radiation is not a perfectly plane wave. At the Brewster angle, the predicted transmittance is 75% at 40 GHz and monotonically increases to 85% at 8 GHz. We have previously measured the transmittance through gratings with larger apertures of 50, 400, and $1500\ \mu\text{m}$, and the results are in good agreement with the theoretical data shown in Fig. 3.⁴ The theoretical calculations (red line) in Fig. 4 are based on the homogenization procedure, Eq. (1), reported in Ref. 2, while the full-wave numerical simulations (black line) are based on the Fourier-Modal-Method (FMM) as implemented in Ref. 10. In the FMM, the field transmitted through the grating is expanded in terms of the diffraction orders of the grating itself and the transmitted power normalized to the incident power (transmittance T) is calculated according to the following formula:

$$T = \frac{n_{inc}}{k_0 n_{out}^2 \cos \vartheta} \sum_m |t_m|^2 \text{Re} \left[\sqrt{n_{out}^2 k_0^2 - \alpha_m^2} \right], \quad (2)$$

where n_{inc} and n_{out} are, respectively, the refractive index of the input and output medium ($n_{in} = n_{out} = 1$ in our case), ϑ is the incident angle of the incoming wave on the grating, t_m is the complex transmission coefficient of the m -th diffracted order, Re indicates the real part, and α_m is the generalized transverse wave-vector: $\alpha_m = k_0 n_{inc} \sin \vartheta + (2m\pi/d)$ $m = 0, \pm 1, \pm 2, \dots$

While the experimental results only span the range of 8–40 GHz, resonant and nonresonant funneling effects span a much broader range. Similar results are expected for both funneling processes up to the frequency where the wavelength of the incident radiation is equal to the period of the grating. Beyond this point, higher order diffraction sets in. However, the period can always be reduced to extend the high frequency range of operation. There is no limit for the low frequency range of nonresonant funneling and it extends all the way to dc frequencies. The lower frequency limit for resonant funneling is set by the thickness of the grating and its ability to contain the lowest order Fabry-Perot mode of

approximately one half wavelength. As seen in Fig. 3, the first order Fabry-Perot mode is at ~ 5 GHz. At very low frequencies of 100 MHz, a zero order transmission mode begins to appear.

These results demonstrate that resonant and nonresonant funneling can operate over a wide range of parameters to enhance the transmission or the absorption even in regions where metals are often considered as perfect conductors. In this paper, we have demonstrated very high transmission at the Brewster angle for an aperture width as small as $\lambda/1500$. Under these extreme conditions, the Brewster angle is at nearly grazing incidence. To date, two methods have been demonstrated to allow the Brewster angle to be adjusted while maintaining the huge field enhancements associated with nonresonant funneling into very small apertures. One method is to rotate the individual metal slats instead of rotating the entire grating.¹¹ With this technique, the Brewster angle has been moved all the way to normal incidence. A second method to vary the nonresonant funneling angle is to use adiabatically tapered slits.¹² Since the Brewster angle is determined by impedance matching at the surface, a wider aperture can be used to vary the acceptance angle and the slit tapered to any size to enhance the fields. In a similar fashion, tapered apertures can make wide angle, broadband absorbers by tapering the slit width to zero.¹³ These results apply to 2D gratings as well. There are numerous other applications for funneling including transparent conductors and antireflective solar collectors. Resonant and nonresonant funneling has also been observed in 1D and 2D acoustic gratings.¹⁴

¹J. A. Porto, F. J. García-Vidal, and J. B. Pendry, *Phys. Rev. Lett.* **83**, 2845 (1999).

²A. Alù, G. D'Aguanno, N. Mattiucci, and M. J. Bloemer, *Phys. Rev. Lett.* **106**, 123902 (2011).

³X. Huang, R. Peng, and R. Fan, *Phys. Rev. Lett.* **105**, 243901 (2010).

⁴N. Aközbe, N. Mattiucci, D. de Ceglia, R. Trimm, A. Alù, G. D'Aguanno, M. A. Vincenti, M. Scalora, and M. J. Bloemer, *Phys. Rev. B* **85**, 205430 (2012).

⁵R. Fan, R. Peng, X. Huang, J. Li, Y. Liu, Q. Hu, M. Wang, and X. Zhang, *Adv. Mater.* **24**, 19806 (2012).

⁶K. Q. Le, C. Argyropoulos, N. Mattiucci, G. D'Aguanno, M. J. Bloemer, and A. Alù, *J. Appl. Phys.* **112**, 094317 (2012).

⁷J. T. Shen, P. B. Catrysse, and S. Fan, *Phys. Rev. Lett.* **94**, 197401 (2005).

⁸A. Pimenov and A. Loidl, *Phys. Rev. B* **74**, 193102 (2006).

⁹M. A. Ordal, R. J. Bell, J. R. W. Alexander, L. L. Long, and M. R. Querry, *Appl. Opt.* **24**, 4493 (1985).

¹⁰L. Li, *J. Opt. Soc. Am. A* **13**, 1870 (1996).

¹¹R. Fan, J. Li, R. Peng, X. Huang, D. Qi, D. Xu, X. Ren, and M. Wang, *Appl. Phys. Lett.* **102**, 171904 (2013).

¹²H. Shen and B. Maes, *Appl. Phys. Lett.* **100**, 241104 (2012).

¹³C. Argyropoulos, K. Q. Le, N. Mattiucci, G. D'Aguanno, and A. Alù, *Phys. Rev. B* **87**, 205112 (2013).

¹⁴G. D'Aguanno, K. Q. Le, R. Trimm, A. Alù, N. Mattiucci, A. D. Mathias, N. Aközbe, and M. J. Bloemer, *Sci. Rep.* **2**, 340 (2012).